Spin Hall effect for polaritons in a transition metal dichalcogenide embedded in a microcavity

Oleg L. Berman, Roman Ya. Kezerashvili, and Yurii E. Lozovik

Phys. Rev. B **99**, 085438 — Published 26 February 2019

DOI: 10.1103/PhysRevB.99.085438

Spin Hall effect for polaritons in a TMDC monolayer embedded in a microcavity

Oleg L. Berman[1,2], Roman Ya. Kezerashvili[1,2], and Yurii E. Lozovik[3,4]
[1] *Physics Department, New York City College of Technology, The City University of New York, Brooklyn, NY 11201, USA*
[2] *The Graduate School and University Center, The City University of New York, New York, NY 10016, USA*
[3] *Institute of Spectroscopy, Russian Academy of Sciences, 142190 Troitsk, Moscow, Russia*
[4] *MIEM at National Research University Higher School of Economics, Moscow, Russia*
(Dated: February 4, 2019)

The spin Hall effect for polaritons (SHEP) in a transition metal dichalcogenides (TMDC) monolayer embedded in a microcavity is predicted. We demonstrate that two counterpropagating laser beams incident on a TMDC monolayer can deflect a superfluid polariton flow due to the generation the effective gauge vector and scalar potentials. The components of polariton conductivity tensor for both non-interacting polaritons without Bose-Einstein condensation (BEC) and for weakly-interacting Bose gas of polaritons in the presence of BEC and superfluidity are obtained. It is shown that the polariton flows in the same valley are splitting: the superfluid components of the A and B polariton flows propagate in opposite directions along the counterpropagating beams, while the normal components of the flows slightly deflect in opposite directions and propagate almost perpendicularly to the beams. The possible experimental observation of SHEP in a microcavity is proposed.

PACS numbers: 72.25.-b, 71.36.+c, 71.35.-y, 71.35.Lk

I. INTRODUCTION

Transition metal dichalcogenides (TMDCs) monolayers such as MoS_2, WS_2, $MoSe_2$, WSe_2, $MoTe_2$, and WTe_2 are characterized by the direct gap in a single-particle spectrum exhibiting the semiconducting band structure and strong spin-orbit coupling[1–7]. Significant spin-orbit splitting in the valence band leads to the formation of two distinct types A and B excitons[8]. A excitons are formed by spin-up electrons from conduction and spin-down holes from valence band, while type B excitons are formed by spin-down electrons from conduction and spin-up holes from valence band[7]. When excitons are created optically, the optical field couples only to the orbital part of the wave function, while the spin is conserved in optical transitions[9]. In the conduction and valence bands of TMDC the electron wave function is given by the linear superposition of p and d orbitals due to the orbital hybridization[10]. Caused by coupling to the optical field, the total angular momentum change between p and d orbitals is 1. The corresponding change of the total moment is compensated by the photon spin 1 due to conservation of the total angular momentum[10].

Recently, microcavity polaritons, formed by excitons in TMDCs embedded in a microcavity, attracted the interest of experimental and theoretical studies. The exciton polaritons, formed by cavity photons and excitons in MoS_2[11] and WS_2[12] monolayers, and a $MoSe_2$ monolayer supported by h-BN layers[13], embedded in a microcavity, were observed experimentally at room temperature. The exciton polariton modes formed due to interaction coupling of excitons in MoS_2 and WS_2 monolayers and microcavity photons were studied[14]. In Ref.[15] the phase diagram of polariton Bose-Einstein condensation (BEC) in a microcavity with an embedded MoS_2 monolayer was presented. An experimentally relevant range of parameters, at which room-temperature superfluidity of exciton polaritons can be observed in a microcavity with an embedded MoS_2 monolayer, was determined in Ref.[16] in the framework of driven diffusive dynamics, while in Ref.[17] the phase diagram of polariton condensate, formed by TMDC excitons coupled to microcavity photons, was studied theoretically.

Strong spin-orbit coupling in TMDCs can lead to the spin Hall effect (SHE), which is one of the most essential effects in spintronics[18,19]. The SHE is the result of generation of a transverse spin current as a response to a longitudinal applied electric field that results in spin accumulation of the carriers with opposite spins at the opposite edges of samples[20–22]. Under applied electric field this transverse spin current can be generated in the systems with strong SOC due either the properties of the electron band structure or scattering on the impurities[20–22].

A method to observe the SHE for cold atoms under light-induced gauge potentials was proposed in Refs.[23–25]. This gauge potential is created when two coordinate dependent laser beams interact with three-level atoms. The vector potential leads to a nonvanishing effective magnetic field, if at least one of the two light beams has a vortex[23,24]. A nonvanishing effective magnetic field can be created without existence of a vortex in a laser beam, if two counterpropagating and overlapping laser beams with shifted spatial profiles interact with three-level atoms[26]. The spin Hall effect for cold atoms can be observed when two counterpropagating Gaussian laser beams with shifted centers generate a spatially slowly varying gauge field acting on three-level atoms[27].

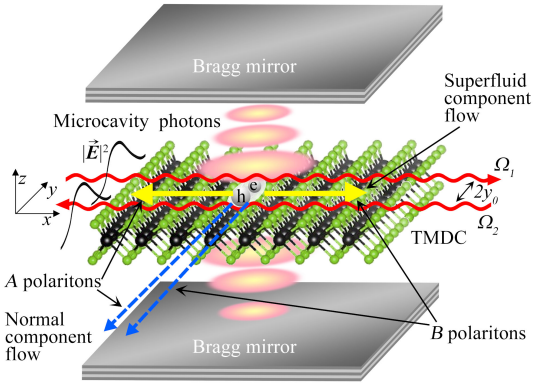

FIG. 1: (Color online) Schematic representation of the light-induced spin Hall effect for polaritons in a TMDC monolayer embedded in a microcavity. The solid and dashed lines with arrows show the directions of deflected superfluid and normal flows of A and B polaritons, correspondingly. Two counterpropagating laser beams are shown by waved lines.

The spin Hall effect for excitons (SHEE) in TMDC was proposed for circularly polarized pumping in Ref.[28], where the mechanism is based on creation of the gauge vector and scalar potentials due to the coupling of excitons to two counterpropagating and overlapping laser beams. The exciton Hall effect (EHE) in TMDC was studied in Ref.[29], where the exciton flows deflect due to the peculiarities of internal structure of TMDC for linearly and circularly polarized pumping. The optical spin Hall effect for microcavity polaritons (OSHEP), formed by excitons in a GaAs quantum well, embedded in a high-quality GaAs/AlGaAs microcavity, caused by the polarization dependence of Rayleigh scattering of light by structural disorder in microcavities, was studied for linearly polarized pumping[30,31].

In this paper we predict the spin Hall effect for polaritons (SHEP), formed by microcavity photons and excitons in TMDC materials embedded into a microcavity. The schematic representation of the light-induced spin Hall effect for microcavity polaritons in a TMDC layer is depicted in Fig. 1 and can be described as follows. Two Bragg mirrors placed opposite each other at the antinodes of the confined photonic mode form a microcavity, and a TMDC layer is embedded parallel to the Brag mirrors within the cavity. As a result of the laser pumping the resonant exciton-photon interaction leads to the Rabi splitting in the excitation spectrum[32,33]. The polaritons cloud is formed due to the coupling of excitons created in a TMDC layer and microcavity photons. The mechanism of the SHEP is following. Two coordinate-dependent, counterpropagating and overlapping laser beams in the plane of the TMDC layer interact with a cloud of polaritons. These laser beams, characterized by Rabi frequencies Ω_1 and Ω_2 produce the spin-dependent gauge magnetic and electric fields[26,27] due to strong SOC for blue electrons and holes in TMDC[28]. Excitons forming polaritons in these gauge magnetic and electric fields form spin-dependent light dressed states[34–36] due to the interaction with laser beams. Below we show that the gauge magnetic field splits the A and B polariton flows. The normal components of the A and B polariton flows slightly deflect in opposite directions and propagate almost perpendicularly to the counterpropagating beams. In contrast, the superfluid components of the A and B polariton flows propagate in opposite directions along the counterpropagating beams. Therefore, one can observe the light-induced spin Hall effect for microcavity polaritons, formed by excitons in a TMDC layer. For the laser pumping frequencies, corresponding to the resonant excitations of one type of excitons (A or B), the corresponding excitons together with coupled to them photons form polaritons, which deflect to only one direction along the counterpropagating beams. The flow of polaritons, associated with this spin current, results in the flow of photons, coupled to excitons in a TMDC layer. Therefore, we propose the method to control photon flows. We are considering the SHEP in two regimes: non-interacting polaritons with the quadratic spectrum in a very dilute limit, when the polariton density is not enough to create BEC at a given temperature and the limit of higher polariton densities in the presence of BEC and superfluidity. Also we propose the method to experimentally observe the superfluidity of microcavity polaritons due to the spin Hall flow of polaritons.

For our study we assume that the pumping beam is circularly polarized, and hence the polaritons are formed by excitons only in one of the valleys: $\mathbf{K}$ or $-\mathbf{K}$[9,37]. Below we focus on formation of polaritons in $\mathbf{K}$ valley and an extension to $-\mathbf{K}$ valley is obvious.

The paper is organized in the following way. In Sec. II, we present the effective Hamiltonian for microcavity polaritons, formed by cavity photons and TMDC excitons, coupled to two laser beams, which is producing the gauge vector and scalar potentials. The tensor of the polariton conductivity, which is the linear response of the polariton flow on the scalar gauge field, and the corresponding resistivity tensor for non-interacting microcavity polaritons in the SHEP regime are obtained in Sec. III. The conductivity tensor for microcavity polaritons in the presence of

superfluidity in the SHEP regime is derived in Sec. IV. In Sec. V, we discuss the possibility to observe the SHEP. The technological applications of the SHEP in TMDC monolayers are considered in Sec. VI. The discussion of our results is presented in Sec. VII. Conclusions follow in Sec. VIII.

II. MICROCAVITY POLARITONS IN THE PRESENCE OF COUNTERPROPAGATING LASER BEAMS

Let us consider the effective Hamiltonian of polaritons, formed by TMDC excitons coupled to microcavity photons in the presence of counterpropagating and overlapping laser beams. The deflection of polaritons occurs via the action of the laser beams on the exciton component of the polaritons. The exciton component of polaritons in a TMDC heterostructure is coupled to two counterpropagating and overlapping coordinate dependent infrared laser beams. The coupling of TMDC excitons to two coordinate dependent laser beams, moving along the plane of TMDC, results in the gauge vector and scalar potentials[26,27], acting on the centers-of-mass of TMDC excitons[28]. The latter causes the spin Hall effect for excitons (SHEE) in TMDC.

The Hamiltonian of TMDC polaritons in the presence of counterpropagating and overlapping laser beams, can be written as

$$\hat{\mathcal{H}} = \hat{H}_{exc} + \hat{H}_{ph} + \hat{H}_{exc-ph} + \hat{H}_{exc-exc}, \tag{1}$$

where $\hat{H}_{exc}$ is the Hamiltonian of excitons in the gauge field produced by two counterpropagating and overlapping laser beams, $\hat{H}_{ph}$ is the Hamiltonian of microcavity photons, $\hat{H}_{exc-ph}$ is the Hamiltonian of exciton-photon coupling, and $\hat{H}_{exc-exc}$ is the Hamiltonian of exciton-exciton interaction.

The Hamiltonian of $2D$ excitons in the presence of counterpropagating and overlapping laser beams can be presented as

$$\hat{H}_{exc} = \sum_{\mathbf{P}} \varepsilon_{ex}(\mathbf{P}) \hat{b}^{\dagger}_{\mathbf{P}} \hat{b}_{\mathbf{P}}, \tag{2}$$

where $\hat{b}^{\dagger}_{\mathbf{P}}$ and $\hat{b}_{\mathbf{P}}$ are excitonic Bose creation and annihilation operators obeying Bose commutation relations. In Eq. (2), $\varepsilon_{ex}(\mathbf{P}) = E_{bg} - E_b + \varepsilon_0(\mathbf{P})$ is the energy dispersion of a single exciton in a TMDC layer, where E_{bg} is the band gap energy, E_b is the binding energy of an exciton, and $\varepsilon_0(\mathbf{P})$ is the energy spectrum of a single exciton in a TMDC coupled to two infrared, coordinate dependent laser beams. The interaction of the exciton in a TMDC monolayer with two counterpropagating Gaussian laser beams can be represented as the interaction with the gauge vector and scalar potentials[28]. We analyze the Hamiltonian for non-interacting TMDC excitons coupled to two counterpropagating Gaussian laser beams in Appendix A. By expanding the gauge vector potential, acting on excitons, in the linear order with respect to the coordinate, the constant gauge magnetic field is obtained. The gauge scalar potential, acting on excitons, is the even function of the coordinate and, therefore, has no linear order term with respect to the coordinate, and, therefore, can be omitted. In this case, $\varepsilon_0(\mathbf{P})$ can be written as[28]

$$\varepsilon_0(\mathbf{P}) = \frac{\left(\mathbf{P} - \mathbf{A}_{\sigma}\right)^2}{2M}, \tag{3}$$

where M is the mass of an exciton and $\mathbf{A}_{\sigma}$ is the gauge vector potential acting on the exciton component of polaritons, associated with different spin states of the conduction band electron, forming an exciton, $\sigma = \uparrow$ and $\downarrow$.

The Hamiltonian of non-interacting photons in a microcavity has the form[38]:

$$\hat{H}_{ph} = \sum_{\mathbf{P}} \varepsilon_{ph}(P) \hat{a}^{\dagger}_{\mathbf{P}} \hat{a}_{\mathbf{P}}, \tag{4}$$

where $\hat{a}^{\dagger}_{\mathbf{P}}$ and $\hat{a}_{\mathbf{P}}$ are photonic creation and annihilation Bose operators. In Eq. (4) $\varepsilon_{ph}(P) = (c/\tilde{n})\sqrt{P^2 + \hbar^2\pi^2 q^2 L_C^{-2}}$ is the spectrum of the microcavity photons, where c is the speed of light, L_C is the length of the cavity, $\tilde{n} = \sqrt{\epsilon}$ is the effective index of refraction of the microcavity, ϵ is the dielectric constant of the cavity, and q is the integer, which represents the longitudinal mode number.

The Hamiltonian of harmonic exciton-photon coupling is given by[39]:

$$\hat{H}_{exc-ph} = \hbar\Omega_R \sum_{\mathbf{P}} \hat{a}^{\dagger}_{\mathbf{P}} \hat{b}_{\mathbf{P}} + h.c.. \tag{5}$$

In Eq. (5) Ω_R is the Rabi splitting constant which represents the exciton-photon coupling energy and is defined by the dipole matrix element, corresponding to the transition with the exciton formation[40] and has different values depending on the material where polaritons are formed.

Below we consider two regimes: i) a very dilute system of non-interacting polaritons when the exciton-exciton interaction is neglected, i. e. $H_{exc-exc} = 0$ and ii) a weakly interacting Bose-gas of polaritons characterized by superfluidity, when exciton-exciton hard core repulsion is taken into account. In this Section we focus on the regime (i), while the regime (ii) is discussed in Sec. IV. Assuming $\hat{H}_{exc-exc} = 0$ the Hamiltonian $\hat{\mathcal{H}}$ can be diagonalized by using the unitary transformation as presented in Appendix B. Substituting Eq. (B3) into (1), one obtains the Hamiltonian of lower polaritons[39]:

$$\hat{\mathcal{H}}_0 = \sum_{\mathbf{P}} \varepsilon_{LP}(\mathbf{P}) \hat{p}^{\dagger}_{\mathbf{P}} \hat{p}_{\mathbf{P}}, \tag{6}$$

where $\hat{p}^{\dagger}_{\mathbf{P}}$ and $\hat{p}_{\mathbf{P}}$ are the Bose creation and annihilation operators for the lower polaritons. The single-particle lower polariton spectrum, which one obtains from Eq. (B2) by substituting (3) and the expression for the spectrum of the microcavity photons, is given by

$$\varepsilon_{LP}(\mathbf{P}) = \hbar\pi q L_C^{-1} - |\hbar\Omega_R| + \varepsilon(\mathbf{P}), \tag{7}$$

where $\varepsilon(\mathbf{P})$ has the form

$$\varepsilon(\mathbf{P}) = \frac{1}{2}\left(\varepsilon_0(\mathbf{P}) + \frac{P^2}{2m_{ph}}\right) = \frac{1}{2}\left(\frac{\left(\mathbf{P} - \mathbf{A}_{\sigma}\right)^2}{2M} + \frac{P^2}{2m_{ph}}\right). \tag{8}$$

In Eq. (8) $m_{ph} = \hbar\pi q/((c/\tilde{n})L_C)$ is the effective mass of microcavity photons, and it is obtained under the assumption of small momenta in the first order with respect to the small parameter $\alpha \equiv 1/2(M^{-1} + (c/\tilde{n})L_C/\hbar\pi q)P^2/|\hbar\Omega_R| \ll 1$.

After simple algebraic transformation Eq. (8) can be rewritten as

$$\varepsilon(\mathbf{P}) = \frac{\left(\mathbf{P} - \mathbf{A}^{(eff)}_{\sigma}\right)^2}{2M_p} + V^{(eff)}, \tag{9}$$

where $M_p = 2\mu$, $\mu = Mm_{ph}/\left(M + m_{ph}\right)$ is the exciton-photon reduced mass. In Eq. (9) $\mathbf{A}^{(eff)}_{\sigma}$ and $V^{(eff)}$ are the effective vector and scalar potentials, respectively, acting on polaritons, and are given by

$$\mathbf{A}^{(eff)}_{\sigma} = \frac{m_{ph}\mathbf{A}_{\sigma}}{M + m_{ph}}, \qquad V^{(eff)} = \frac{A^2_{\sigma}}{4\left(M + m_{ph}\right)}. \tag{10}$$

In Eq. (10) $\mathbf{A}_{\sigma}$ is the gauge vector potential acting on excitons, obtained in Ref.[28] and given by Eq. (A4). Let us mention that $\mathbf{A}^{(eff)}_{\sigma}$ and $V^{(eff)}$ are obtained employing diagonalization of the Hamiltonian $\hat{\mathcal{H}}$ under assumption $\hat{H}_{exc-exc} = 0$ by using the unitary transformation presented in Appendix B. It follows from Eq. (10) that acting on polaritons effective gauge scalar potential $V^{(eff)}$, determined by the gauge vector potential $\mathbf{A}_{\sigma}$ acting on excitons, depends on y, while the gauge scalar potential V_{σ} acting on excitons in the linear order with respect to y is a constant. Therefore, $V^{(eff)}$ leads to non-zero effective gauge electric field $\mathbf{E}^{(eff)}$ acting on polaritons. In contrast, the gauge electric field acting on excitons is zero in the linear order with respect to y.

Substituting Eq. (A4) into (10), assuming slowly changing gauge potential, and keeping only terms, linear with respect to y, the effective gauge vector and scalar potentials acting on the polaritons can be written as

$$\mathbf{A}^{(eff)}_{\sigma} = \frac{m_{ph}\eta_{\sigma}\hbar\left(|k_1| + |k_2|\right)}{2\left(M + m_{ph}\right)}\left(1 + \frac{y}{2l}\right)\mathbf{e}_x, \quad V^{(eff)} = \frac{\hbar^2\left(|k_1| + |k_2|\right)^2}{16\left(M + m_{ph}\right)}\left(1 + \frac{y}{l}\right). \tag{11}$$

Therefore, the effective gauge magnetic $\mathbf{B}^{(eff)}_{\sigma}$ and electric fields $\mathbf{E}^{(eff)}$ fields acting along z- and y-axis, respectively, are

$$\mathbf{B}^{(eff)}_{\sigma} = \nabla_{\mathbf{R}} \times \mathbf{A}^{(eff)}_{\sigma} = \frac{-\eta_{\sigma}\hbar m_{ph}\left(|k_1| + |k_2|\right)}{4l\left(M + m_{ph}\right)}\mathbf{e}_z, \quad \mathbf{E}^{(eff)} = -\nabla_{\mathbf{R}} V^{(eff)} = -\frac{\hbar^2\left(|k_1| + |k_2|\right)^2}{16l\left(M + m_{ph}\right)}\mathbf{e}_y. \tag{12}$$

The analysis of Eqs. (11) and (12) shows that the effective gauge vector potential and effective magnetic field are different for A and B polaritons due to the factor $\eta_{\uparrow} = 1$ for an A exciton and $\eta_{\downarrow} = -1$ for a B exciton, while the

effective gauge scalar potential and effective electric field do not depend on the spin orientation σ. As a result, the effective gauge magnetic field $\mathbf{B}_{\sigma}^{(eff)}$ deflects the polaritons consisting from the excitons with different spin states of charge carriers (A and B excitons) towards opposite directions. Thus, the system under consideration demonstrates the SHEP. Also as mentioned above, there is an effective uniform electric field acting on polaritons, in contrast to absence of such uniform field for excitons.

Let us mention that the SHEE was proposed for interlayer excitons in a $MoSe_2 - WSe_2$ van der Waals heterostructure, where electrons are located in a $MoSe_2$ monolayer, while holes are located in a WSe_2 monolayer[28]. The interlayer excitons in such heterostructures are characterized by relatively high lifetime, due to suppression of the electron-hole recombination since electrons and holes are spatially separated in different monolayers[41,42]. However, the increase of the exciton lifetime does not essentially influence the lifetime of polaritons, because the polariton lifetime is determined by the lifetime of the microcavity photons. The lifetime of the microcavity photons is much smaller than the lifetime of excitons, since the microcavity photons leave the microcavity much faster than electrons and hole recombine. Therefore, one can consider the excitons in a single TMDC monolayer, embedded in a microcavity, without sufficient decrease of the polariton lifetime compared with the TMDC van der Waals heterostructure.

III. RESISTIVITY AND CONDUCTIVITY TENSORS FOR NON-INTERACTING MICROCAVITY POLARITONS IN THE SHEP REGIME

In this Section, we consider the dilute system of non-interacting microcavity polaritons when the concentration n is too low to form the BEC at given temperature. Applying the Drude model, one can write the transport equation for microcavity polaritons, moving in both the effective electric $\mathbf{E}^{(eff)}$ and magnetic $\mathbf{B}_{\sigma}^{(eff)}$ fields as[43,44]

$$\frac{d\mathbf{P}}{dt} = \mathbf{E}^{(eff)} + \mathbf{v} \times \mathbf{B}_{\sigma}^{(eff)} - \frac{\mathbf{P}}{\tau}, \tag{13}$$

where $\mathbf{v}$ is the velocity and τ is a scattering time of microcavity polaritons. For a steady state, setting $d\mathbf{P}/dt = 0$, and using $\mathbf{P} = M_p\mathbf{v}$, one obtains

$$\mathbf{E}^{(eff)} = \frac{M_p}{n\tau}\mathbf{j} - \frac{\mathbf{j} \times \mathbf{B}_{\sigma}^{(eff)}}{n}, \tag{14}$$

where the linear polariton flow density is defined as $\mathbf{j} = n\mathbf{v}$.

Following Ref.[44], for the resistivity and conductivity tensors for polaritons moving in effective electric and magnetic fields we use the similar definitions. In particular, the 2×2 resistivity matrix ϱ_{σ} can be defined as $\mathbf{E}^{(eff)} = \varrho_{\sigma}\mathbf{j}$, with the diagonal $\rho_{\sigma xx}$ and $\rho_{\sigma yy}$, and the off-diagonal $\rho_{\sigma xy}$ and $\rho_{\sigma yx}$ components known as the Hall resistivity[43] given by

$$\rho_{\sigma xx} = \rho_{\sigma yy} = \frac{M_p}{n\tau}, \quad \rho_{\sigma xy} = -\rho_{\sigma yx} = \frac{\eta_{\sigma} B^{(eff)}}{n}, \tag{15}$$

where $B^{(eff)}$ is the magnitude of the effective magnetic field $\mathbf{B}_{\sigma}^{(eff)}$.

We define the Hall coefficient $R_{H\sigma}$ as

$$R_{H\sigma} = \frac{\rho_{\sigma yx}}{B^{(eff)}} = -\frac{\eta_{\sigma}}{n}. \tag{16}$$

The conductivity tensor $\tilde{\sigma}_{\sigma}$ is defined as the inverse matrix to the resistivity matrix ϱ_{σ}. In our case of the Hall conductivity, the diagonal and off-diagonal components of $\tilde{\sigma}_{\sigma}$ are given by

$$\sigma_{\sigma xx} = \sigma_{\sigma yy} = \frac{\sigma_0}{1 + \omega_c^2\tau^2}, \quad \sigma_{\sigma xy} = -\sigma_{\sigma yx} = -\frac{\eta_{\sigma}\sigma_0\omega_c\tau}{1 + \omega_c^2\tau^2}, \tag{17}$$

where $\sigma_0 = \tau n/M_p$ and $\omega_c = B^{(eff)}/M_p$ is the cyclotron frequency. As it can be seen from Eqs. (15), (16), and (17), the Hall resistivity, Hall coefficient, and Hall conductivity depend on the spin orientation σ.

The x and y components of the linear polariton flow density are defined as $j_x = -\sigma_{\sigma xy}E^{(eff)}$ and $j_y = -\sigma_{\sigma yy}E^{(eff)}$.

The dependencies of the cyclotron frequency ω_c on the distance between the centers of the contrpropagated laser beams for A and B polaritons are presented in Fig. 2. According to Fig. 2, one can conclude that the cyclotron frequency ω_c decreases with the parameter l, and it is the largest for a WS_2 monolayer and the smallest for a $MoSe_2$ monolayer at the same l. Also, for the same TMDC monolayer ω_c is larger for B polaritons than for A polaritons.

In our calculations and estimations we use the following parameters. For the microcavity we use the parameters from Ref.[13]: $\tilde{n} = 2.2$, $L_C = 2.3$ μm, $q = 5$ and obtain the effective mass of microcavity photons: $m_{ph} = 5.802 \times 10^{-6} m_0$,

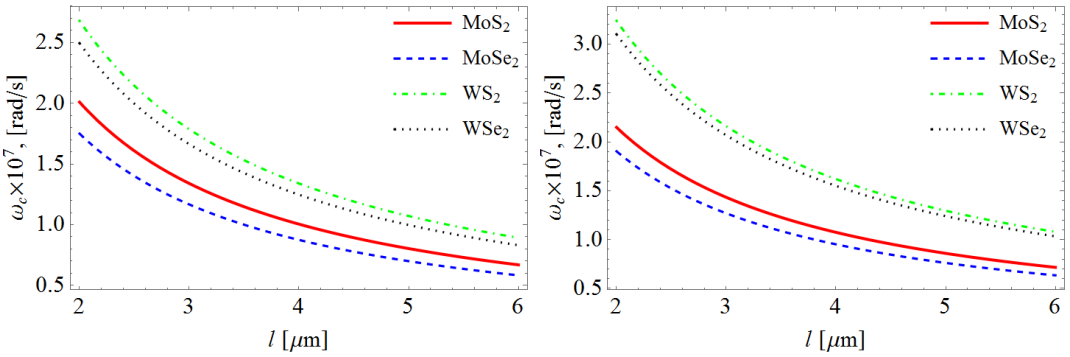

FIG. 2: (Color online) The dependence of the cyclotron frequency ω_c on the parameter l, determined by the distance between the counterpropagating laser beams. Calculations performed for $|k_1| + |k_2| = 3\ \mu\text{m}^{-1}$. (a) and (b) ω_c as a function of l for A and B polaritons, respectively.

where m_0 is the mass of an electron. The experimentally measured values of the Rabi splitting constant $\hbar\Omega_R$ were reported as 46 ± 3 meV[11], 20 meV[13], and 70 meV[12] for MoS_2, $MoSe_2$, and WS_2 monolayers, respectively. We use the sets of effective masses for electrons and holes in various TMDCs from Refs.[45,46].

The scattering time of microcavity polaritons is $\tau(P) = X_{\mathbf{P}}^{-4}\tau_{ex}(P) \approx 4\tau_{ex}(P)$[47], where $X_{\mathbf{P}}$ is defined by Eq. (B4). The exciton relaxation time $\tau_{ex}(P)$ can be approximated by its average value $\bar{\tau}_{ex} = \langle\tau_{ex}(P)\rangle$, which can be obtained from the exciton mobility $\tilde{\mu}_{ex} = e\bar{\tau}_{ex}/M$. For a WSe_2 monolayer the exciton relaxation time was measured as $\bar{\tau}_{ex} = 260$ fs[48]. Therefore, a scattering time of microcavity polaritons can be estimated as $\tau = 4\bar{\tau}_{ex} = 1.040$ ps, which is less than the polariton lifetime estimated as tens of picoseconds[33]. In our calculations we use this value for the scattering time of microcavity polaritons τ.

According to Ref.[28], for the SHEE the cyclotron frequency is $\omega_c \sim 1/M$, where M is the mass of the exciton. For the SHEP According to Eq. (12) for polaritons $B^{(eff)} \sim m_{ph}/(M + m_{ph})$. Since $m_{ph} \ll M$ we have $M_p \approx m_{ph}$, and one concludes that for the SHEP cyclotron frequency is also $\omega_c \sim 1/M$. Therefore, the cyclotron frequencies for the SHEP and the SHEE will be almost the same order of magnitude, and the degree to which spin currents are separated in the case of exciton-polaritons will be approximately the same as in the regular exciton case.

IV. SPIN HALL EFFECT FOR MICROCAVITY POLARITONS IN THE PRESENCE OF SUPERFLUIDITY

In the dilute limit $na_{2D}^2 \ll 1$, where a_{2D} is the 2D exciton Bohr radius, at sufficiently low temperatures the Bose-Einstein condensation of polaritons appears in the system, and the corresponding Hamiltonian of a weakly-interacting Bose gas of microcavity polaritons with hard-core repulsion is presented, for example, in Ref.[49]. For the simplicity one can consider the Thomas-Fermi approximation for the polariton condensate density profile in the non-quantizing effective magnetic field $\mathbf{B}_\sigma^{(eff)}$. Within this approximation the polariton condensate density profile for the system does not depend on the effective magnetic field. The Thomas-Fermi approximation is valid if the healing length ξ[50] of polaritons is much less than the other characteristic length parameters of the system such as the effective magnetic length: $\xi \ll r_B^{(eff)}$. The healing length for polaritons ξ is given by $\xi = \hbar/\sqrt{2M_p\mu_p}$, where μ_p is the chemical potential of weakly-interacting Bose gas of polaritons in the Bogoliubov approximation[51,52] $\mu_p = U_{\text{eff}}^{(0)} n$, where $U_{\text{eff}}^{(0)}$ is the Fourier transform of the effective polariton-polariton pair repulsion potential, given by the hard-core contact potential. In Ref.[49] $U_{\text{eff}}^{(0)}$ is defined as $U_{\text{eff}}^{(0)} = 3ke^2a_{2D}/(2\epsilon)$, where $k = 9 \times 10^9\ \text{N}\cdot\text{m}^2/\text{C}^2$, $\epsilon = \tilde{n}^2$ is the dielectric constant of the microcavity, and $a_{2D} = \hbar^2\epsilon/\left(2\mu_{ex}ke^2\right)$ is the 2D exciton Bohr radius, and μ_{ex} is the exciton reduced mass, defined as $\mu_{ex} = m_{e\uparrow}m_{h\downarrow}/(m_{e\uparrow} + m_{h\downarrow})$ and $\mu_{ex} = m_{e\downarrow}m_{h\uparrow}/(m_{e\downarrow} + m_{h\uparrow})$ for A and B excitons, correspondingly.

In experiments, the exciton density in a TMDC monolayer was obtained up to $n = 5 \times 10^{11}\ \text{cm}^{-2}$[53], and we use this value for n in our estimations. Since 2D Bohr radius is $a_{2DA} = 3.875$ Å and $a_{2DB} = 4.41$ Å for A and B excitons, respectively, one correspondingly obtains $na_{2DA}^2 = 7.509 \times 10^{-4} \ll 1$ and $na_{2DB}^2 = 9.723 \times 10^{-4} \ll 1$. Therefore, the polariton system can be treated as a weakly-interacting Bose gas. We estimate the healing length as $\xi_A = 1.947\ \mu$m and $\xi_B = 1.825\ \mu$m for A and B polaritons, respectively. The corresponding effective magnetic lengths can be estimated as $r_{BA}^{(eff)} = 1.236$ mm and $r_{BB}^{(eff)} = 1.124$ mm. Therefore, $\xi_A \ll r_{BA}^{(eff)}$ and $\xi_B \ll r_{BB}^{(eff)}$ for A and B polaritons, respectively, and the Thomas-Fermi approximation is valid for the system under consideration.

The Bogoliubov approximation for the dilute weakly-interacting Bose gas of polaritons results in the sound spectrum

of collective excitations at low momenta[51,52]: $\varepsilon(P) = c_S P$ with the sound velocity[49]: $c_S = \left(U_{\rm eff}^{(0)} n/M_p\right)^{1/2} = \left(3ke^2 a_{2D} n/(2\epsilon M_p)\right)^{1/2}$. Let us consider the microcavity polaritons at low temperatures in the presence of superfluidity when the effective magnetic $\mathbf{B}_\sigma^{(eff)}$ and electric $\mathbf{E}^{(eff)}$ fields are given by Eqs. (12). In the presence of superfluidity, the polariton system has two components: superfluid and normal[51,52]. The superfluid-normal phase transition in this 2D system is the Kosterlitz-Thouless transition[54], and the temperature of this transition T_c in a 2D microcavity polariton system is determined as:

$$T_c = \frac{\pi\hbar^2 n_s(T_c)}{2k_B M_p} \, , \tag{18}$$

where $n_s(T)$ is the concentration for the superfluid component of the polariton system[51,52] in a microcavity as a function of temperature T, and k_B is the Boltzmann constant.

The polaritons in the superfluid component do not collide, and therefore, the scattering time of microcavity polaritons is $\tau \to +\infty$. In this case, one obtains the transport equation for microcavity polaritons from Eq. (13), which can be rewritten for the x- and y-components as

$$M_p \frac{dv_x}{dt} = -\eta_\sigma B^{(eff)} v_y, \qquad M_p \frac{dv_y}{dt} = E^{(eff)} + \eta_\sigma B^{(eff)} v_x. \tag{19}$$

If the initial conditions for Eq. (19) are $v_{0x} = v_{0y} = 0$, the superfluid polaritons will be accelerated until the system reaches steady state, which corresponds to $dv_x/dt = dv_y/dt = 0$. According to Eq. (19), in the steady state $v_y = 0$ and $v_x = -E^{(eff)}/\eta_\sigma B^{(eff)}$. Defining the linear superfluid polariton flow density as $\mathbf{j}^{(s)} = n_s \mathbf{v}$, one obtains the conductivity tensor $\tilde{\sigma}_\sigma^{(s)}(T)$ for the superfluid with the following components:

$$\sigma_{\sigma xx}^{(s)} = \sigma_{\sigma yy}^{(s)} = 0, \qquad \sigma_{\sigma xy}^{(s)}(T) = -\sigma_{\sigma yx}^{(s)}(T) = -\frac{n_s(T)}{\eta_\sigma B^{(eff)}} \, . \tag{20}$$

For the conductivity tensor $\tilde{\sigma}_\sigma^{(n)}(T)$ for the normal component one can use Eq. (17), substituting $\sigma_0(T) = \tau n_n(T)/M_p$, where $n_n(T)$ is a 2D concentration of the normal component[51,52]. The total conductivity tensor in the presence of superfluidity is given by $\tilde{\sigma}_\sigma^{(tot)}(T) = \tilde{\sigma}_\sigma^{(s)}(T) + \tilde{\sigma}_\sigma^{(n)}(T)$.

Following the procedure[51] we obtain the superfluid density as $n_s(T) = n - n_n(T)$ by determining the density of the normal component $n_n(T)$ as a linear response of the total momentum with respect to the external velocity:

$$n_n(T) = \frac{3\zeta(3)}{2\pi\hbar^2} \frac{k_B^3 T^3}{c_S^4 M_p} \, . \tag{21}$$

Since the diagonal components of the conductivity tensor for the superfluid component $\sigma_{\sigma xx}^{(s)} = \sigma_{\sigma yy}^{(s)}$ equal to zero, only the normal component contributes to the diagonal components of the total conductivity tensor $\sigma_{\sigma xx}^{(tot)} = \sigma_{\sigma yy}^{(tot)} = \sigma_{\sigma xx}^{(n)} = \sigma_{\sigma yy}^{(n)}$. In the presence of superfluidity at $T < T_c$ the diagonal components of the total conductivity tensor are directly proportional to the concentration of the normal component $n_n(T)$. The latter increases according to Eq. (21) as T^3. Thus one can determine $n_n(T)$ and $n_s(T)$ by a measurement of $\sigma_{\sigma xx}^{(tot)}$ or $\sigma_{\sigma yy}^{(tot)}$ at different temperatures at $T < T_c$. At $T \geq T_c$ the concentration of the normal component equals to the total concentration of polaritons. Therefore, by the measurement of the diagonal components of the total conductivity tensor, one can determine the Kosterlitz-Thouless phase transition temperature T_c.

Let us mention that the components of the conductivity tensor can be obtained via the linear polariton flow density $\mathbf{j}$, which is defined by the polariton flow. The polariton flow is determined by the component of the total polariton momentum $\mathbf{P}_\parallel$ in the direction parallel to the Bragg mirrors. The component $\mathbf{P}_\parallel$ can be calculated from the experimental measurement of the angular intensity distribution of the photons escaping the optical microcavity, similar to the experiment suggested in Ref.[47]. The polariton flow was obtained experimentally recording directly the momentum distribution of the particles by angle resolving the far-field photon emission from the polaritons, because $\mathbf{P}_\parallel$ has a one-to-one correspondence with the external angle of photon emission, which was measured[55]. Also the polariton flow can be obtained by using the first order spatial correlation function for a polariton condensate, which was measured experimentally by employing a Michelson interferometer setup[56,57].

Since at the Kosterlitz-Thouless transition temperature $T = T_c$ the universal jump in the superfluid concentration occurs[54], one can determine T_c by observation of the jumps at $T = T_c$ in $\sigma_{\sigma xx}^{(tot)}(T)$ and $\sigma_{\sigma xy}^{(tot)}(T)$ components of the total conductivity tensor as functions of temperature T. This is possible, because the coefficients of proportionality in

the dependencies of $\sigma^{(n)}_{\sigma xy}(T)$ and $\sigma^{(s)}_{\sigma xy}(T)$ on $n_n(T)$ and $n_s(T)$, correspondingly, are different. Besides, only the normal concentration $n_n(T)$ contributes to $\sigma^{(n)}_{\sigma xx}(T)$ and $\sigma^{(n)}_{\sigma yy}(T)$. Also by observation of $\sigma_{\sigma xx}$ and $\sigma_{\sigma xy}$ one can determine a scattering time of microcavity polaritons τ by using Eq. (17). Our calculations show that the contribution to $\sigma^{(tot)}_{\sigma xy}(T)$ and therefore the Hall linear polariton flow density is mainly given by the superfluid component, while the contribution from the normal component is negligible.

Substituting Eq. (21) for the density n_s of the superfluid component into Eq. (18), one obtains an equation for the Kosterlitz-Thouless transition temperature T_c. The solution of this equation is

$$T_c = \left[\left(1 + \sqrt{\frac{32}{27} \left(\frac{M_p k_B T_c^0}{\pi \hbar^2 n} \right)^3 + 1} \right)^{1/3} - \left(\sqrt{\frac{32}{27} \left(\frac{M_p k_B T_c^0}{\pi \hbar^2 n} \right)^3 + 1} - 1 \right)^{1/3} \right] \frac{T_c^0}{2^{1/3}} \, , \tag{22}$$

where T_c^0 is the temperature, corresponding to vanishing superfluid density in the mean-field approximation, when $n_s(T_c^0) = 0$,

$$T_c^0 = \frac{1}{k_B} \left(\frac{\pi \hbar^2 n c_s^4 M_p}{6\zeta(3)} \right)^{1/3} \, . \tag{23}$$

At the temperature $T = 300$ K for A polaritons we have obtained the total Hall linear polariton flow density in the presence of superfluidity $j_x^{(tot)} = 8.51887 \times 10^{13}$ nm^{-1}s^{-1}, $j_x^{(tot)} = 9.54342 \times 10^{13}$ nm^{-1}s^{-1}, $j_x^{(tot)} = 9.76334 \times 10^{13}$ nm^{-1}s^{-1}, $j_x^{(tot)} = 1.1415 \times 10^{14}$ nm^{-1}s^{-1} for WSe_2 for MoS_2, $MoSe_2$, and WSe_2, respectively. At the temperature $T = 300$ K for B polaritons we have obtained the total Hall linear polariton flow density in the presence of superfluidity $j_x^{(tot)} = 1.22581 \times 10^{14}$ nm^{-1}s^{-1}, $j_x^{(tot)} = 1.32831 \times 10^{14}$ nm^{-1}s^{-1}, $j_x^{(tot)} = 1.09252 \times 10^{14}$ nm^{-1}s^{-1}, $j_x^{(tot)} = 1.19047 \times 10^{14}$ nm^{-1}s^{-1} for MoS_2, $MoSe_2$, and WSe_2, respectively. Therefore, for A polaritons the total Hall linear polariton flow density is the largest for a WSe_2 monolayer and the smallest for a MoS_2 monolayer, while for B polaritons it is the largest for a $MoSe_2$ monolayer and the smallest for a WS_2 monolayer. Also, $j_x^{(tot)}$ for B polaritons is larger than for A polaritons for the same monolayer.

Let us mention that the results, presented in this Section, are applicable for A and B polaritons. A polaritons are formed via A excitons coupled to microcavity photons, and B polaritons are formed via B excitons coupled to microcavity photons, correspondingly. The effective masses of A and B excitons in a TMDC heterostructure are given by $M_A = m_{e\uparrow} + m_{h\downarrow}$ and $M_B = m_{e\downarrow} + m_{h\uparrow}$, where $m_{e\uparrow(\downarrow)}$ is the effective mass of spin-up (spin-down) electrons from the conduction band and $m_{h\uparrow(\downarrow)}$ is the effective mass of spin-up (spin-down) holes from the valence band, correspondingly. In our formulas above we assume that for A and B excitons mass M should be replaced by M_A and M_B, respectively. Correspondingly, the polariton effective mass M_p should be replaced by M_{pA} and M_{pB} for A and B polaritons, respectively.

V. ON THE OBSERVATION OF SHEP

The observation of the SHEP in TMDC is related to the measurement of the shift of the angular distribution of the photons escaping the optical microcavity due to the effective gauge magnetic and electric fields acting on polaritons. In the absence of the effective gauge magnetic and electric fields, the angular distribution of the photons escaping the microcavity is central-symmetric with respect to the perpendicular to the Bragg mirrors. In order to analyze the deflection of the polariton flow in the (x, y) plane of the microcavity due to the SHEP one can measure the average tangent of the angle α of deflection for the polariton flow, defined as

$$\overline{\tan \, \alpha} = \left| \frac{j_x}{j_y} \right| = \left| \frac{\sigma_{\sigma xy}}{\sigma_{\sigma yy}} \right| . \tag{24}$$

At the absence of superfluidity by substituting Eq. (17) into Eq. (24) one obtains $\overline{\tan \, \alpha} = \omega_c \tau$. The same expression is valid in the presence of superfluidity for the angle of deflection of the flow of the normal component, since

$$\overline{\tan \, \alpha^{(n)}} = \left| \frac{j_x^{(n)}}{j_y^{(n)}} \right| = \left| \frac{\sigma^{(n)}_{\sigma xy}}{\sigma^{(n)}_{\sigma yy}} \right| = \omega_c \tau. \tag{25}$$

Substituting $l = a^2/8y_0$, $a = 10$ μm, $y_0 = 2.5$ μm, $|k_1| + |k_2| \approx 3$ μm^{-1}, $\tau = 1.040$ ps into Eq. (25), one can estimate for WSe_2, $\overline{\tan \, \alpha^{(n)}} \approx 10^{-5}$, and $\overline{\alpha^{(s)}} \approx 10^{-3}$ [0]. Therefore, the normal component of the polariton system almost does not deflect in the direction perpendicular to the effective gauge electric field due to the SHEP.

The average tangent of the angle $\alpha^{(s)}$ of deflection of the flow of the superfluid component can be obtained as

$$\overline{\tan\ \alpha^{(s)}} = \left|\frac{j_x^{(s)}}{j_y^{(s)}}\right| = \left|\frac{\sigma_{\sigma xy}^{(s)}}{\sigma_{\sigma yy}^{(s)}}\right| \to +\infty, \tag{26}$$

because $\sigma_{\sigma yy}^{(s)} = 0$ according to Eq. (20). Therefore, one has $\overline{\alpha^{(s)}} = 90^0$ for the average angle of deflection of the superfluid component due to the SHEP.

Since the cyclotron frequency ω_c for polaritons is the same by the order of magnitude as for excitons $\omega_c \sim 1/M$ and a scattering time of microcavity polaritons $\tau \sim 10^{-12}$ s, the deflection of the normal component of polariton flow is very small, but is different for A and B polaritons. In contract, as one can see from Eqs. (20) and (26) that $\overline{\alpha^{(s)}} \to 90^0$ and is the same for all different TMDC monolayers embedded in different microcavities. Therefore, due to the SHEP the A and B polariton flows are splitting. The normal components of the A and B polariton flows are slightly deflected in opposite directions and propagate almost perpendicularly to the counterpropagating beams. In contrast, the superfluid components of the A and B polariton flows are propagated in opposite directions along the counterpropagating beams. Thus, one can separate the superfluid and normal components of the polariton flow. Therefore, by measuring the angular distribution of the photons escaping the optical microcavity in the presence and absence of the effective gauge magnetic and electric fields and determining the shift of these distributions, one can observe the SHEP.

Note that the cause of the shift of the angular distribution of the photons escaping from the superfluid component due to the SHEP is different from the reason of the shift of the angular distribution of the photons escaping from the normal component in the polariton drag effect[47,58]. This difference is related to the fact that the drag effect is caused only by the excitations, while the gauge fields can influence the entire superfluid component.

VI. POSSIBLE TECHNOLOGICAL APPLICATIONS OF SHEP

We propose the optical switch based on microcavity polaritons, formed by excitons in a TMDC monolayer, in the SHEP regime. We propose the switch for a polariton flow. We consider the polariton system in the presence of superfluidity. Using circular polarized pumping, one can excite both A and B excitons in one valley simultaneously. In this case, A and B polaritons are formed due to coupling of A and B excitons to the microcavity photons, correspondingly. Due to the SHEP, there will be two different by magnitude superfluid spin Hall polariton flows perpendicular to the effective gauge electric field in opposite directions for A and B polaritons. We can control these two different superfluid polariton flows by changing the concentration of excited A and/or B polaritons. A polariton flow occurs also in the direction along the effective gauge electric field.

Besides, one can excite either A or B polaritons once at the time. We can switch the magnitude and direction of superfluid polariton Hall flow perpendicular to the effective gauge electric field by switching the frequency of laser pumping, exciting either A or B polaritons. By switching from the regime of A excitons (or A polaritons) to B excitons (or B polaritons) or vise versa, we can switch the direction of superfluid polariton Hall flow to the opposite one and change the magnitude of superfluid polariton Hall flow. However, the magnitude of this superfluid polariton flow will be different for A and B polaritons. This magnitude of the superfluid polariton flow can be controlled by exciting either A or B polaritons.

VII. DISCUSSION

Another important feature of the SHEP in TMDC is that the conductivity tensor $\tilde{\sigma}$ depends on the exciton mass M, which is different for A and B excitons. Therefore, the conductivities and polariton flows (including Hall conductivities and Hall flows) will have different magnitudes for A and B polaritons. Besides, the Hall polariton flows have different directions for A and B polaritons, since they depend on the spin orientation factor η_σ. The SHEP in TMDC differs for A and B polaritons by twofold: i. the polaritonic flow has different magnitudes due to the different masses of A and B polaritons; ii. the Hall polariton flows will have different directions for A and B polaritons, since they depend on the spin orientation factor.

The SHEP can be observed for both linear and circular polarized light pumping. For linear polarized light the excitons, forming polaritons, are created in both valleys $\mathbf{K}$ and $-\mathbf{K}$. In this case A polaritons from valley $\mathbf{K}$ and B polaritons from the $-\mathbf{K}$ valley will be deflected in one direction, while the B polaritons from the valley $\mathbf{K}$ and A polaritons from the valley $-\mathbf{K}$ will be deflected in opposite direction. For left circular polarized light A and B polaritons from the valley $\mathbf{K}$ will be deflected in opposite directions. Analogously, for right circular polarized light A and B polaritons from the valley $-\mathbf{K}$ will be deflected in opposite directions.

Let us mention that the EHE in monolayer MoS_2 and valley-selective spatial transport of excitons on a micrometre scale were directly observed by polarization-resolved photoluminescence mapping[29]. This EHE studied in Ref.[29] is caused by intrinsic properties of a TMDC material. While the EHE is very important for valleytronics, the proposed SHEP is caused by the properties of two external counterpropagating laser beams, and, therefore, can be controlled by changing the parameters of these laser beams. The study the possibilities of application of the EHE[29] for microcavity polaritons will be performed in subsequent work.

Let us discuss at this point the difference of the SHEP and OSHEP[30,31]. The SHEP and the OSHEP[30,31] have two cardinally different mechanisms. In the OSHEP the deflection of polaritons appears due to the deflection of the photon component of polaritons. The OSHEP was analyzed for polaritons, formed by excitons in a GaAs quantum well, embedded in a high-quality GaAs/AlGaAs microcavity[31]. The OSHEP is controlled by the linear polarization of the laser pump[30,31]. In contrast, in the SHEP in TMDC the deflection of polaritons appears due to the deflection of the exciton component of polaritons. The SHEP in TMDC appears due coupling of two spatially varying infrared laser beams to the internal levels of the excitons in TMDC, considered for excitons in Ref.[28]. If under linear polarized pumping required for OSHEP[30,31], both valleys would be populated, the polaritons corresponding to the, for example, $\mathbf{K}$ valley A excitons and $-\mathbf{K}$ valley A excitons would deflect to different edges of cavity. In contract, for the SHEP in TMDC the circular polarized pumping, which creates excitons in only one chosen valley, allows to initiate separated Hall polariton flows of A and B polaritons from the same valley in opposite directions. The latter allows to control the spin Hall effect in a chosen valley, which is very useful for valleytronics. Since elastic scattering of photons by disorder is the main scattering mechanism required for the OSHEP[30,31], in the case of weak disorder in TMDC the SHEP proposed in our paper is the dominant effect, because the SHEP is not caused by disorder. Moreover, since the SHEP can be observed for both circular and linear polarized light pumping, in the latter case one can modulate the signals from two counterpropagating laser beams either by changing periodically the distance l between two laser beams or by a rotating screen with a hole in front of the source of two laser beams. In this case, when the signals from two laser beams are off, the SHEP is absent and only the OSHEP is present, while in the presence of the signals from two laser beams the both SHEP and OSHEP are present. The latter allows one to analyze the contribution from SHEP to the defected flow of photons, escaping the microcavity. By this way the SHEP can be registered as the modulated component of the signal. Another essential difference between the SHEP and OSHEP is that the SHEP provides the deflection of polariton superfluid component, while the OSHEP does not result in deflection of the polariton superfluid component due to the absence of the scattering of superfluid component by disorder.

The novel 2D materials such as transition metal dichalcogenides [1], germanene[59,60], and stanene[61] are characterized by relatively large exciton binding energies and strong spin-orbit coupling. However, in contrast to TMDC, germanene and stanene demonstrate high exciton binding energies and strong SOC only under strong perpendicular electric field. We assume that the SHEP can occur for microcavity polaritons, formed by excitons only in the novel 2D materials such as either TMDCs or germanene and stanene under high perpendicular electric field due to strong SOC. In contrast the SHEP cannot be observed for microcavity polaritons, formed by excitons in a semiconductor quantum well due to absence of strong SOC. Let us mention that while we study exciton polaritons formed by excitons in TMDCs, our approach seems to be applicable for all novel 2D materials with strong SOC, including germanene and stanene under high electric field.

Let us emphasize the importance of considered in this paper spin Hall effect for polaritons. By using the SHEP, one can control the flows of photons, and induced by SHEP the flows of polaritons lead to flows of photons, escaping the microcavity. So we suggest the method to control photon flows. Another advantage of consideration of SHEP is the possibility of observation of spin Hall effect in the superfluid system.

VIII. CONCLUSIONS

We have proposed the spin Hall effect for microcavity polaritons, formed by excitons in a TMDC and microcavity photons. We demonstrated that the polariton flow can be achieved by generation the effective gauge vector and scalar potentials, acting on polaritons. We have obtained the components of polariton conductivity tensor for both non-interacting polaritons without BEC and for weakly-interacting Bose gas of polaritons in the presence of BEC and superfluidity. These results for non-interacting polaritons are applicable for the two-component system of A and B polaritons. We have studied the SHEP for both superfluid and normal components. Let us emphasize that induced by SHEP the flows of polaritons lead to flows of photons, escaping the microcavity. Therefore, one can control the flows of photons. Another advantage of of SHEP is the possibility of observation of spin Hall effect in the superfluid system. For circular polarized light we demonstrated that due to the SHEP the polariton flows in the same valley are splitting: the normal component of the A and B polariton flows slightly deflect in opposite directions and propagate almost perpendicularly to the counterpropagating beams, while the superfluid components of the A and B polariton flows propagate in opposite directions along the counterpropagating beams. Thus, one can separate the superfluid

and normal components of the polariton flow. Since only the superfluid component contributes to the polariton Hall flow, while the normal component contributes only to the flow almost parallel to the effective gauge electric field, the SHEP can be employed to separate the superfluid component from the normal component. For the linear polarized light one can observe the same effect for the A and B polariton flows in $\mathbf{K}$ and $-\mathbf{K}$ valleys, respectively. Observation of the SHEP in the presence of superfluidity can be achieved by measuring the angles $\alpha^{(n)}$ and $\alpha^{(s)}$ of deflections for the normal and superfluid polariton flows.

Acknowledgments

O. L. B. and R. Ya. K. were supported by US Department of Defense under Grant No. W911NF1810433 and PSC CUNY under Grant No. 60599-00 48. Yu. E. L. was supported by Program of Basic Research of National Research University HSE and by the RFBR Grant (17-02-01134).

Appendix A: The Hamiltonian for a TMDC exciton coupled to two counterpropagating Gaussian laser beams

We consider two infrared laser beams linearly polarized along the y axis, which propagate along the x axis, acting on the TMDC excitons, forming polaritons. The exciton ground state $|g\rangle \equiv |1s\rangle$ and two low excited states $|1\rangle \equiv |2p_y\rangle$ and $|2\rangle \equiv |3p_y\rangle$ were under consideration in Ref.[28]. These two laser beams couple $|g\rangle$ to $|1\rangle$ and $|2\rangle$, correspondingly, with equal detuning δ. Two counterpropagating Gaussian laser beams are characterized by symmetrical centers, shifted along the y axis, and spatial profiles $eE_{1(2)}(\mathbf{R})\langle g|\mathbf{e}_y \cdot \mathbf{r}|1(2)\rangle/\hbar = \Omega_{1(2)}(\mathbf{R})e^{i\phi_{1(2)}(\mathbf{R})}$, where e is the electron charge, $E_{1(2)}(\mathbf{R})$ is the external electric field, $\mathbf{R} = (x, y)$ is the coordinate vector of the center-of-mass of an exciton, $\Omega_1 = \Omega_0 \exp\left[-(y - y_1)^2/a^2\right]$ and $\Omega_2 = \Omega_0 \exp\left[-(y - y_2)^2/a^2\right]$ are Rabi frequencies that characterized the beams, $y_1 = -y_2 = y_0$, $\phi_1(\mathbf{R}) = k_1 x$, $\phi_2(\mathbf{R}) = k_2 x$.

The effective center-of-mass Hamiltonian H_σ for an exciton, associated with different spin states of the conduction band electron, forming an exciton, $\sigma =\uparrow$ and $\sigma =\downarrow$, in a TMDC coupled to two coordinate dependent laser beams is given by[28]

$$H_\sigma = \frac{1}{2M}\left(\mathbf{P} - \mathbf{A}_\sigma\right)^2 + V_\sigma, \tag{A1}$$

where $\mathbf{P}$ is the momentum of the center-of-mass of an exciton, $M = m_e + m_h$ is the exciton total mass (m_e and m_h are the effective masses of an electron and a hole in TMDC, respectively, V_σ and $_\sigma$ are the spin-dependent gauge scalar and vector potential, correspondingly, which depend on $\mathbf{R}$. The effective gauge magnetic field $\mathbf{B}_\sigma$ is defined as $\mathbf{B}_\sigma = \nabla_{\mathbf{R}} \times \mathbf{A}_\sigma$. Two counterpropagating Gaussian laser beams with the centers, shifted along the y axis, produce a coordinate dependent gauge field $\mathbf{B}_\sigma$[28]:

$$\mathbf{A}_\sigma = \frac{\eta_\sigma \hbar\left(|k_1| + |k_2|\right)}{1 + e^{-y/l}}\mathbf{e}_x, \qquad \mathbf{B}_\sigma = \frac{-\eta_\sigma \hbar\left(|k_1| + |k_2|\right)}{4l\cosh^2(y/2l)}\mathbf{e}_z, \tag{A2}$$

where $\eta_\uparrow = 1$ and $\eta_\downarrow = -1$ for A and B excitons, respectively, $l = a^2/8y_0$, $a = 10$ μm is the beam width, $y_0 = 2.5$ μm is the spatial shift of two laser beams, $|k_1| + |k_2| \approx 3$ μm^{-1}.

Below we provide the qualitative analysis for the validity of the assumption that the exciton gauge magnetic field $\mathbf{B}_\sigma(y)$ given by Eq. (A4) and scalar potential $V_\sigma(y)$ can be treated as coordinate independent constants. The aforementioned assumption is valid, if y is small compared with l ($l = 5$ μm[28]) and $y \ll \tilde{y}(y)$, where $\tilde{y}(y)$ is the characteristic length of changes in the exciton gauge magnetic field and scalar potential, defined as

$$\tilde{y}(y) = \left|\frac{B(y)}{dB(y)/dy}\right| = \left|\frac{V_\sigma}{dV_\sigma(y)/dy}\right| = \frac{l}{\tanh\left(\frac{y}{2l}\right)}, \tag{A3}$$

where $B(y) = |\mathbf{B}_\sigma(y)|$. Assuming that y does not exceed 2.5 μm[28], one obtains $\tilde{y}(y) \geq \tilde{y}\,(2.5\ \mu\text{m}) = 20.41$ μm. Therefore, since at $y \leq 2.5$ μm the inequality $y \ll \tilde{y}(y)$ together with the assumption about small y compared with l hold, we assume that in our system the exciton gauge magnetic field $\mathbf{B}_\sigma(y)$ given by Eq. (A4) and scalar potential $V_\sigma(y)$ do not depend on coordinates and, therefore, are constants.

Assuming $y/l \ll 1$ at $y \ll 5$ μm, we expand $\mathbf{A}_\sigma$ and $\mathbf{B}_\sigma$ in series in terms of y/l and in the first order approximation obtain from Eq. (A2) the following:

$$\mathbf{A}_\sigma = \frac{\eta_\sigma \hbar\left(|k_1| + |k_2|\right)}{2}\left(1 + \frac{y}{2l}\right)\mathbf{e}_x, \qquad \mathbf{B}_\sigma = \frac{-\eta_\sigma \hbar\left(|k_1| + |k_2|\right)}{4l}\mathbf{e}_z, \tag{A4}$$

The spin-dependent gauge scalar potential V_σ is given by[28]:

$$V_\sigma(\mathbf{R}) = \lambda_\sigma + W(\mathbf{R}), \tag{A5}$$

where

$$\lambda_\downarrow = \hbar\delta, \qquad \lambda_\uparrow \approx \hbar\delta + \frac{\hbar\Omega^2}{4\delta}, \tag{A6}$$

and $\Omega \equiv \left(\Omega_1^2 + \Omega_2^2\right)^{1/2}$. Then one obtains from Eq. (A6) the following expression:

$$\lambda_\uparrow \approx \hbar\delta + \frac{\hbar\Omega_0^2}{2\delta} e^{-2y_0^2/a^2} e^{-2y^2/a^2} \cosh(y/2l). \tag{A7}$$

In Eq. (A5), the scalar potential $W(\mathbf{R})$ is given by

$$W(\mathbf{R}) = \frac{\hbar^2}{2M}\left(|\nabla_{\mathbf{R}}\theta|^2 + \sin^2\theta\cos^2\theta\,|\nabla_{\mathbf{R}}\phi(\mathbf{R})|^2\right), \tag{A8}$$

where $\theta = \tan^{-1}(\Omega_1/\Omega_2)$, $\phi(\mathbf{R}) \equiv \phi_1(\mathbf{R}) - \phi_2(\mathbf{R})$. From Eq. (A8) the following expression can be derived

$$W(\mathbf{R}) = \frac{\hbar^2}{2M}\left(\frac{4y_0^2}{a^4} + \frac{\left(|k_1| + |k_2|\right)^2}{4}\right)\frac{1}{\cosh^2(y/2l)}. \tag{A9}$$

Since we consider two counterpropagating Gaussian laser beams with symmetrically shifted centers along the y axis[28], we used for derivation of Eq. (A9), the following relation: $|k_1 - k_2| = |k_1| + |k_2|$. Assuming $y/l \ll 1$ at $y \ll 5$ μm, in the first order with respect to y/l, one obtains $W = \text{const}$. Therefore, in our approach we will not consider the gauge scalar potential acting on excitons, since in the first order with respect to y/l it results in zero scalar gauge field, because the nonzero scalar potential occurs only in the second order on y/l.

Appendix B: Diagonalization of the Hamiltonian $\hat{\mathcal{H}}$ by using unitary transformation

We apply the quasilocal approximation which can be used for the momenta P, obeying to the condition $Pr_B^{(eff)} \gg \hbar$, where $r_B^{(eff)} = \sqrt{\hbar/B^{(eff)}}$ is the effective magnetic length, and $B^{(eff)}$ is the magnitude of the effective magnetic field, acting on polaritons, defined by Eq. (12). In this quasiclassical approach the coordinate y, entering the exciton energy dispersion $\varepsilon_{ex}(\mathbf{P})$ through the gauge vector potential $\mathbf{A}_\sigma$, is considered to be a number parameter rather than an operator.

If one assumes $\hat{H}_{exc-exc} = 0$, the Hamiltonian $\hat{\mathcal{H}}$ can be diagonalized by using unitary transformation and can be written as[39]:

$$\hat{H}_0 = \sum_{\mathbf{P}} \varepsilon_{LP}(\mathbf{P})\hat{p}_{\mathbf{P}}^\dagger \hat{p}_{\mathbf{P}} + \sum_{\mathbf{P}} \varepsilon_{UP}(\mathbf{P})\hat{u}_{\mathbf{P}}^\dagger \hat{u}_{\mathbf{P}}, \tag{B1}$$

where $\hat{p}_{\mathbf{P}}^\dagger$ and $\hat{u}_{\mathbf{P}}^\dagger$, and $\hat{p}_{\mathbf{P}}$ and $\hat{u}_{\mathbf{P}}$ are the Bose creation and annihilation operators for the lower and upper polaritons, correspondingly. The energy spectra of the lower and upper polaritons are given by

$$\varepsilon_{LP/UP}(\mathbf{P}) = \frac{\varepsilon_{ph}(P) + \varepsilon_{ex}(\mathbf{P})}{2} \mp \frac{1}{2}\sqrt{(\varepsilon_{ph}(P) - \varepsilon_{ex}(\mathbf{P}))^2 + 4|\hbar\Omega_R|^2}, \tag{B2}$$

where the Rabi splitting between the upper and lower states at $P = 0$ equals $2\Omega_R$.

The operators of excitons and photons are defined as[39]

$$\hat{b}_{\mathbf{P}} = X_{\mathbf{P}}\hat{p}_{\mathbf{P}} - C_{\mathbf{P}}\hat{u}_{\mathbf{P}}, \qquad \hat{a}_{\mathbf{P}} = C_{\mathbf{P}}\hat{p}_{\mathbf{P}} + X_{\mathbf{P}}\hat{u}_{\mathbf{P}}, \tag{B3}$$

where $X_{\mathbf{P}}$ and $C_{\mathbf{P}}$ are[39]

$$X_{\mathbf{P}} = \frac{1}{\sqrt{1 + \left(\frac{\hbar\Omega_R}{\varepsilon_{LP}(\mathbf{P}) - \varepsilon_{ph}(P)}\right)^2}}, \qquad C_{\mathbf{P}} = -\frac{1}{\sqrt{1 + \left(\frac{\varepsilon_{LP}(\mathbf{P}) - \varepsilon_{ph}(P)}{\hbar\Omega_R}\right)^2}}, \tag{B4}$$

and $|X_{\mathbf{P}}|^2$ and $|C_{\mathbf{P}}|^2 = 1 - |X_{\mathbf{P}}|^2$ point out the exciton and cavity photon fractions in the lower polariton[39].

At $\alpha \equiv 1/2(M^{-1} + (c/\tilde{n})L_C/\hbar\pi q)P^2/|\hbar\Omega_R| \ll 1$ we obtain from Eq. (B4) the following relation: $X_{\mathbf{P}} \approx 1/\sqrt{2}$.

[1] A. Kormányos, G. Burkard, M. Gmitra, J. Fabian, V. Zólyomi, N. D. Drummond, and V. Fal'ko, 2D Mater. **2**, 022001 (2015).
[2] K. F. Mak, C. Lee, J. Hone, J. Shan, and T. F. Heinz, Phys. Rev. Lett. **105**, 136805 (2010).
[3] K. F. Mak, K. He, J. Shan, and T. F. Heinz, Nat. Nanotechnol. **7**, 494 (2012).
[4] L. Britnell, R. M. Ribeiro, A. Eckmann, R. Jalil, B. D. Belle, A. Mishchenko, Y.-J. Kim, R. V. Gorbachev, T. Georgiou, S. V. Morozov, A. N. Grigorenko, A. K. Geim, C. Casiraghi, A. H. Castro Neto, and K. S. Novoselov, Science **340**, 1311 (2013).
[5] J. S. Ross, S. Wu, H. Yu, N. J. Ghimire, A. M. Jones, G. Aivazian, J. Yan, D. G. Mandrus, D. Xiao, W. Yao, and X. Xu, Nat. Commun. **4**, 1474 (2013).
[6] W. Zhao, Z. Ghorannevis, L. Chu, M. Toh, C. Kloc, P.-H. Tan, and G. Eda, ACS Nano **7**, 791 (2013).
[7] G. Wang, A. Chernikov, M. M. Glazov, T. F. Heinz, X. Marie, T. Amand, and B. Urbaszek, Rev. Mod. Phys. **90**, 021001 (2018).
[8] T. C. Berkelbach, M. S. Hybertsen, and D. R. Reichman, Phys. Rev. B **88**, 045318 (2013).
[9] D. Xiao, G. B. Liu, W. Feng, X. Xu, and W. Yao, Phys. Rev. Lett. **108**, 196802 (2012).
[10] H. Shi, H. Pan, Y.-W. Zhang, and B. I. Yakobson, Phys. Rev. B **87**, 155304 (2013).
[11] X. Liu, T. Galfsky, Z. Sun, F. Xia, E.-C. Lin, Y.-H. Lee, S. Kéna-Cohen, and V. M. Menon, Nature Photonocs **9**, 30 (2015).
[12] L. C. Flatten, Z. He, D. M. Coles, A. A. P. Trichet, A. W. Powell, R. A. Taylor, J. H. Warner, and J. M. Smith, Sci. Rep. **6**, 33134 (2016).
[13] S. Dufferwiel, S. Schwarz, F. Withers, A. A. P. Trichet, F. Li, M. Sich, O. Del Pozo-Zamudio, C. Clark, A. Nalitov, D. D. Solnyshkov, G. Malpuech, K. S. Novoselov, J. M. Smith, M. S. Skolnick, D. N. Krizhanovskii, and A. I. Tartakovskii, Nature Commun. **6**, 8579 (2015).
[14] M. I. Vasilevskiy, D. G. Santiago-Pérez, C. Trallero-Giner, N. M. R. Peres, and A. Kavokin, Phys. Rev. B **92**, 245435 (2015).
[15] N. Lundt, A. Maryński, E. Cherotchenko, A. Pant, X. Fan, S. Tongay, G. Sek, A. V. Kavokin, S. Höfling, and C. Schneider, 2D Mater. **4**, 015006 (2017).
[16] G. V. Kolmakov, L. M. Pomirchi, and R. Ya. Kezerashvili, J. Opt. Soc. Am. B **33**, C72 (2016).
[17] K. H. Lee, C. Lee, H. Min, and S. B. Chung, Phys. Rev. Lett. **120**, 157601 (2018).
[18] I. Žutić, J. Fabian, and S. Das Sarma, Rev. Mod. Phys. **76**, 323 (2004).
[19] M. Eschrig, Rep. Prog. Phys. **78**, 104501 (2015).
[20] M. I. Dyakonov and V. I. Perel, JETP Lett. **13**, 467 (1971).
[21] J. E. Hirsch, Phys. Rev. Lett. **83**, 1834 (1999).
[22] S. Zhang, Phys. Rev. Lett. **85**, 393 (2000).
[23] G. Juzeliunas and P. Öhberg, Phys. Rev. Lett. **93**, 033602 (2004).
[24] G. Juzeliunas, P. Öhberg, J. Ruseckas, and A. Klein, Phys. Rev. A **71**, 053614 (2005).
[25] G. Juzeliunas, J. Ruseckas, and P. Öhberg, J. Phys. B **38**, 4171 (2005).
[26] G. Juzeliunas, J. Ruseckas, P. Öhberg, and M. Fleischhauer, Phys. Rev. A **73**, 025602 (2006).
[27] S. L. Zhu, H. Fu, C. J. Wu, S. C. Zhang, and L. M. Duan, Phys. Rev. Lett. **97**, 240401 (2006).
[28] Y.-M. Li, J. Li, L.-K. Shi, D. Zhang, W. Yang, and K. Chang, Phys. Rev. Lett. **115**, 166804 (2015).
[29] M. Onga, Y. Zhang, T. Ideue, and Y. Iwasa, Nature Materials **16**, 1193 (2017).
[30] A. Kavokin, G. Malpuech, and M. Glazov, Phys. Rev. Lett. **95**, 136601 (2005).
[31] C. Leyder, M. Romanelli, J. Ph. Karr, E. Giacobino, T. C. H. Liew, M. M. Glazov, A. V. Kavokin, G. Malpuech, and A. Bramati, Nature Physics **3**, 628 (2007).
[32] I. Carusotto and C. Ciuti, Rev. Mod. Phys. **85**, 299 (2013).
[33] *Universal Themes of Bose-Einstein Condensation*, edited by N. Proukakis, D. W. Snoke, and P. B. Littlewood (Cambridge University Press, 2017).
[34] J. H. Shirley, Phys. Rev. **138**, B979 (1965).
[35] Ya. B. Zel'dovich, Sov. Phys. JETP **24**, 1006 (1967).
[36] H. Sambe, Phys. Rev. A **7**, 2203 (1973).
[37] K. F. Mak, K. He, C. Lee, G. H. Lee, J. Hone, T. F. Heinz, and J. Shan, Nature Materials **12**, 207 (2013).
[38] S. Pau, G. Björk, J. Jacobson, H. Cao and Y. Yamamoto, Phys. Rev. B **51**, 14437 (1995).
[39] C. Ciuti, P. Schwendimann, and A. Quattropani, Semicond. Sci. Technol. **18** S279 (2003).
[40] V. Savona, C. Piermarocchi, A. Quattropani, P. Schwendimann, and F. Tassone, Phase Transitions **68 (1)**, 169 (1999).
[41] Yu. E. Lozovik and V. I. Yudson, Sov. Phys. JETP **44**, 389 (1976).
[42] Yu. E. Lozovik, Phys. Uspekhi **188**, N 11 (2018) (in print).
[43] S. H. Simon, *The Oxford Solid State Basics* (Oxford University Press, Oxford, 2013).
[44] D. W. Snoke, *Solid State Physics: Essential Concepts* (Addison-Wesley, San Francisco, 2009).
[45] A. Kormanyos, V. Zolyomi, N. D. Drummond, and G. Burkard, Phys. Rev. X **4**, 011034 (2014).
[46] I. Kylänpää and H.-P. Komsa, Phys. Rev. B **92**, 205418 (2015).

[47] O. L. Berman, R. Ya. Kezerashvili, and Yu. E. Lozovik, Phys. Rev. B **82**, 125307 (2010).
[48] F. Cadiz, C. Robert, E. Courtade, M. Manca, L. Martinelli, T. Taniguchi, K. Watanabe, T. Amand, A. C. H. Rowe, D. Paget, B. Urbaszek, and X. Marie, Appl. Phys. Lett. **112**, 152106 (2018).
[49] O. L. Berman, Yu. E. Lozovik, and D. W. Snoke, Phys. Rev. B **77**, 155317 (2008).
[50] L. Pitaevskii and S. Stringari, *Bose-Einstein Condensation* (Clarendon Press, Oxford, 2003).
[51] A. A. Abrikosov, L. P. Gorkov and I. E. Dzyaloshinski, *Methods of Quantum Field Theory in Statistical Physics* (Prentice-Hall, Englewood Cliffs. N.J., 1963).
[52] A. Griffin, *Excitations in a Bose-Condensed Liquid* (Cambridge University Press, Cambridge, England, 1993).
[53] Y. You, X.-X. Zhang, T. C. Berkelbach, M. S. Hybertsen, D. R. Reichman, and T. F. Heinz, Nature Physics. **11**, 477 (2015).
[54] J. M. Kosterlitz and D. J. Thouless, J. Phys. C **6**, 1181 (1973); D. R. Nelson and J. M. Kosterlitz, Phys. Rev. Lett. **39**, 1201 (1977).
[55] B. Nelsen, G. Liu, M. Steger, D. W. Snoke, R. Balili, K. West, and L. Pfeiffer, Phys. Rev. X **3**, 041015 (2013).
[56] G. Roumpos, M. Lohse, W. H. Nitsche, J. Keeling, M. H. Szymańska, P. B. Littlewood, A. Löffler, S. Höfling, L. Worschech, A. Forchel, and Y. Yamamoto, Proc. Natl. Acad. Sci. U.S.A. **109**, 6467 (2012).
[57] D. Caputo, D. Ballarini, G. Dagvadorj, C. S. Muñoz, M. De Giorgi, L. Dominici, K. West, L. N. Pfeiffer, G. Gigli, F. P. Laussy, M. H. Szymanska, and D. Sanvitto, Nature Materials **17**, 145 (2018).
[58] O. L. Berman, R. Ya. Kezerashvili, and Yu. E. Lozovik, Physics Letters A **374**, 3681 (2010).
[59] C. J. Tabert and E. J. Nicol, Phys. Rev. B **89**, 195410 (2014).
[60] Z. Ni, Q. Liu, K. Tang, J. Zheng, J. Zhou, R. Qin, Z. Gao, D. Yu, and J. Lu, Nano Lett. **12**, 113 (2012).
[61] S. Saxena, R. P. Chaudhary, and S. Shukla, Sci. Rep. **6**, 31073 (2016).